Atmos. Chem. Phys. Discuss., 13, 31363–31407, 2013
www.atmos-chem-phys-discuss.net/13/31363/2013/
doi:10.5194/acpd-13-31363-2013

Atmospheric Chemistry and Physics Discussions

Systematic comparison of dust BSC-DREAM8b modeled profiles with Potenza EARLINET lidar database

L. Mona[1], N. Papagiannopoulos[1], S. Basart[2], J. Baldasano[2,3], I. Binietoglou[1], C. Cornacchia[1], and G. Pappalardo[1]

[1]Istituto di Metodologie per l'Analisi Ambientale (CNR-IMAA), C. da S. Loja, 85050 Tito Scalo, Potenza, Italy
[2]Barcelona Supercomputing Center, Barcelona, Spain
[3]Environmental Modelling Laboratory, Technical University of Catalonia, Barcelona, Spain

Received: 13 September 2013 – Accepted: 11 November 2013 – Published: 2 December 2013

Correspondence to: L. Mona (mona@imaa.cnr.it)

Published by Copernicus Publications on behalf of the European Geosciences Union.

Abstract

In this paper, we report the first systematic comparison between dust extinction profiles forecasted by a model and measured by a Raman lidar. We use the BSC-DREAM8b model, one of the most widely used dust regional models in the Mediterranean, and Potenza EARLINET lidar profiles for Saharan dust cases, the largest one-site database of dust extinction profiles. A total of 310 dust cases were compared for the May 2000–July 2012 period. The model well reconstructs the measured layering: profiles are correlated within 5 % of significance for 60 % of the cases and the dust layer center of mass as measured by lidar and modeled by BSC-DREAM8b differ on average 0.3 ± 1.0 km. Cases with a dust optical depth lower than 0.1 account for 70 % of uncorrelated profiles. Although the good agreement in terms of profile shape and extinction value order of magnitude, the comparison with extinction profiles measured by the Raman lidar shows that BSC-DREAM8b typically underestimate the dust extinction coefficient in particular below 3.5 km and for low concentrations and overestimates the occurrence of dust layer top height above 15 km.

1 Introduction

Atmospheric aerosols are both of natural (sea salt, forest fires smoke, wind-risen soil dust, volcanic dust and biological debris) and anthropogenic (industrial activities, fossil fuel processes, and so forth) origin. A major component of atmospheric aerosol is mineral dust, originated through wind erosion of the land surface in arid and semiarid regions. The main sources of mineral dust are the Saharan desert, the desert areas of Saudi Arabia and eastern Asia. At global scale, desert dust has the largest source strength of all aerosol types (Zender et al., 2004), accounting for the 75 % of the global aerosol mass (Kinne et al., 2006). The source strength depends critically on the wind speed and the turbulent state of the boundary layer as well as local soil properties (Zender et al., 2003). The size of particles varies from 100 µm near the source and

ACPD
13, 31363–31407, 2013

decreases with the distance from the source. During dust episodes over the Saharan desert, dust particles can travel over long distances crossing the North Atlantic Ocean and reaching Scandinavia (Franzen et al., 1994) and the south-eastern United States (Prospero et al., 2002) or travel eastwards and even as far as China (Tanaka et al., 2005).

Desert dust particles have many effects. They can impact climate, precipitation cycle, ecosystems and human health. Dust interacts directly with the solar incoming and terrestrial outgoing radiation by absorption and scattering. The absorption/scattering pattern of dust ranges along with its variable nature (Alfaro et al., 2004; Mishra and Tripathi, 2008; Redmond et al., 2010). Furthermore, dust emission fluxes are sensitive to climatic changes, thus there is indication of negative (or positive) climate feedback via dust-climate forcing (Carslaw et al., 2010; Schulz et al., 2012). Dust can act as cloud condensation (CCN) and ice nucleii (Sassen et al., 2003; Klein et al., 2010; Smoydzin et al., 2012) and as much initiate the cloud formation and evolution processes. Furthermore Saharan dust over the oceans, by supplying iron and phosphorus, promotes nitrogen fixation and hence oceanic primary productivity (Mills et al., 2004; Sañudo-Wilhelmy and Flegal, 2003; Gallisai et al., 2012). This causes CO_2 absorption, dimethylsulfide release and production of cloud condensation nuclei in the marine troposphere and so can promote cooling of the atmosphere (Henriksson et al., 2000).

A number of medical conditions can be attributed to desert dust particles; recently the attention is drawn to the health impact of the wind-blown particles. Over the last decades, epidemiological studies have identified a link between pollution of airborne particles and health hazards such as respiratory and cardiovascular diseases (e.g Kwon et al., 2002; Pérez et al., 2009; De Longueville et al., 2013). Poor air quality due to desert dust intrusions is observed and documented by many studies (e.g., Querol et al., 2009). European countries have adopted air quality standards for airborne particulate matter, in particular there is a strong need for dust forecasting in South Europe, due to the vicinity to the Saharan desert. The European Directive 2008/50/CE allows subtraction of PM exceedances caused by natural events from models and statistics

ACPD
13, 31363–31407, 2013

used (European Commission, 2011) to determine air quality of EU sites. At the present time, there are only few studies addressing the issue of the effective determination of desert dust contribution to particulate matter (PM) measurements on systematic basis (Basart et al., 2012b; Gobbi et al., 2007; Escudero et al., 2007; Pederzoli et al., 2010; Querol et al., 2009; Sanchez et al., 2007).

The vertical distribution of aerosol is of particular importance because it is a combined signature of atmospheric transport patterns, residence times in the atmosphere, and the efficiency of the vertical exchange. Therefore plays a crucial role in the complex aerosol-cloud interaction and in the radiation equilibrium of the atmosphere. While passive ground-based (e.g., AERONET) or space-borne observations (e.g. MODIS, MISR or OMI) have been used to evaluate the 2-D distribution of particles, the vertical distribution cannot be evaluated by these instruments. Lidar techniques are capable of identifying, locating, and characterizing aerosols in the vertical. Nowadays lidars have attained a high degree of reliability and have been used by regional networks to produce long-term, self-consistent, and well-calibrated measurements of aerosol properties. At European level, long term quality-assured measurements of aerosol optical properties profiles are provided since May 2000 by the European Aerosol Research Lidar Network (EARLINET) (www.earlinet.org) (Bosenberg et al., 2003), a coordinated network of stations that make use of advanced lidar methods for the vertical profiling of aerosols.

Lidar observations have been widely used for investigating atmospheric desert dust. An overview is provided by Mona et al. (2012a). The intrusion into the Planetary Boundary Layer (PBL) of desert dust and mixing processes of dust with other aerosol types can be investigated in detail using the vertical profiling capability of lidars (e.g. Muller et al., 2003; Hara et al., 2009; Mona et al., 2012b). Long-range transport of dust can be monitored and tracked by ground-based lidar networks or spaceborne lidars (e.g. Ansmann et al., 2003; Papayannis et al., 2008; Liu et al., 2008; Schuster et al., 2012). Lidar measurements in combination with other techniques are ideal to investigate certain aspects of atmospheric composition, transport, and deposition of aerosol (e.g. Ferrare

ACPD
13, 31363–31407, 2013

et al., 1998, 2001). Furthermore, profiling capability permits the simultaneous detection of aerosol layers and clouds and the investigation of aerosol/cloud interactions (e.g. Ansmann et al., 1992; Hart et al., 2005; Sakai et al., 2003; Sassen et al., 2003; Vaughan et al., 2009). The lidar/radar synergistic approach is a novel and promising research field in this context (McGill et al., 2004).

Because of these aspects, the Sand and Dust Storm Warning Advisory and Assessment System (SDS-WAS) programme established in 2007 by the World Meteorological Organization (WMO) stimulates and promotes lidar activities for dust investigations at international level (WMO report, 2011). With respect to lidar activities the following actions are foreseen for the next 5 yr (WMO report, 2011): coordination of the observational networks, integration between other instruments, near real time data delivery, and evaluation/assimilation of models. In particular, comparison and assimilation of observations with models are fundamental for improving dust forecast, revealing weaknesses of individual models and providing an assessment of uncertainties in simulating the dust cycle.

This paper reports for the first time a systematic comparison between lidar profiles of dust optical properties and modeled extinction dust profiles in terms of geometrical features and optical properties. The BSC-DREAM8b dust regional model (Nickovic et al., 2001; Pérez et al., 2006a, b; Basart et al., 2012a) is used for this study. This model is operated in the Barcelona Supercomputer Center (BSC, www.bsc.es) and is one of the most widely used models for dust investigation over European region (e.g. Amiridis et al., 2009; Gobbi et al., 2013). Up to now there are few examples of comparison between ground-based lidar and modeled profiles (e.g. Ferrare et al., 2006). Raw data from the space-borne CALIOP (Cloud-Aerosol Lidar with Orthogonal Polarization) lidar (Winker et al., 2009) where used for evaluating the results from a global chemical and transport model (GEOS-Chem) (Generoso et al., 2008; Ford and Heald, 2012). Koffi et al. (2012) evaluated the capability of 12 models to reproduce the vertical distribution of aerosols observed at global scale by CALIOP. However this comparison is affected by the uncertainties on CALIOP extinction retrieval due to assumptions on lidar ratio

ACPD
13, 31363–31407, 2013

values needed for the retrieval that seems to be more critical for dust cases (Amiridis et al., 2013). Based mainly on Raman lidars, EARLINET represents a reference point for more common backscatter lidars (and ceilometers) and for the first satellite-borne lidar, CALIOP. Raman lidar technique allows the direct measurement of the aerosol extinction profile and the independent aerosol backscatter profile measurement. The ratio of these two quantities, namely the lidar ratio (S), is a quantity that: (i) does not depend on the amount of aerosol, (ii) depends on intensive aerosol properties as dimension, chemical composition, refractive index, (iii) is a quantity needed for assumptions necessary for aerosol optical properties retrieval in case of elastic backscatter lidar measurements. Based mainly on Raman lidars, EARLINET is therefore a reference network for aerosol typing and for improving optical properties retrieval in backscatter lidar as CALIOP.

For a systematic comparison with dust modeled extinction profile, lidar profiles measured by the Potenza EARLINET station are considered as pilot case. Potenza station has been selected because it has at the present the longest and widest database of Saharan dust aerosol optical properties profiles. Data used for this first comparison are introduced in Sect. 2. Section 3 describes the methodology developed for the lidar vs. BSC-DREAM8b dust extinction profiles comparison in terms of layering and optical properties. Results of the systematic comparison are reported in Sect. 4. Finally conclusions are reported in Sect. 5.

2 Data used

2.1 Potenza-EARLINET lidar data

For this study, vertical profiles of aerosol optical properties, as measured – at CNR-IMAA Atmospheric Observatory (CIAO), Potenza, Southern Italy (40°36′ N, 15°44′ E, 760 m a.s.l.), are considered. Potenza station is particularly interesting for the Saharan dust investigation because it has collected the greatest amount of observations on Sa-

ACPD
13, 31363–31407, 2013

haran dust particles among the EARLINET sites. This is due to the fact that Potenza has been participating in the network since its beginning, and the station is located in the central region of the Mediterranean Basin affected by many dust events originated in Western, Central and Eastern Sahara. A previous study performed on 3 yr of dust profiles collected by EARLINET demonstrates that stations located in the Central Mediterranean are the most affected by dust within the network with a large variability of dust conditions in terms of aerosol load, aerosol layer altitude range and optical properties (Papayannis et al., 2008). In addition Potenza is an EARLINET core station, because is equipped with a multi-wavelength Raman lidar system (Mona et al., 2009).

For the aims of this study, we considered all vertical profiles identified as related to dust cases, and therefore belonging to the desert dust category of the EARLINET database as at June 2013. The period covered is May 2000–July 2012. During this period, the Potenza EARLINET lidar (PEARL) followed some upgrades: the system was an elastic/Raman lidar operating at 355 nm with a further elastic channel at 532 nm when EARLINET started on 2000 and it is now a multi-wavelength Raman + depolarization lidar (Mona et al., 2009; Madonna et al., 2011). This kind of lidar is nowadays the state-of-the-art lidar for atmospheric aerosol study and is able to measure 3 backscatter (355, 532 and 1064 nm), 2 extinction (355 and 532 nm) and the particle linear depolarization ratio at 532 nm. From these independent measurements it is possible in some circumstances obtaining information on aerosol microphysical properties through specific numerical algorithms (Böckmann et al., 2005; Müller et al., 2004; Osterloh et al., 2009; Veselovskii et al., 2012; Wagner et al., 2013). Simultaneous measurements of all these optical properties are also particularly interesting for aerosol typing (Mona et al., 2012b).

Since May 2000, the Potenza EARLINET station has been performing measurements following the EARLINET schedule for observations. Measurements are performed at each station on a regular schedule of one daytime measurement per week around noon (when there is a well developed boundary layer) and two night-time measurements per week (Raman extinction measurements), when the signal-to-noise Ra-

ACPD
13, 31363–31407, 2013

man signal is higher (Bösenberg et al., 2003; Matthias et al., 2004). Additional measurements are performed in agreement with EARLINET specific strategy designed for the exploitation of CALIOP measurements (Pappalardo et al., 2010). Besides these measurements planned disregarding the specific aerosol content, further EARLINET coordinated observations are addressed to monitor special events such as Saharan dust outbreaks, forest fires, photochemical smog and volcanic eruptions. For dust events, alerts are diffused by the NTUA (National Technical University of Athens) group to all network stations 24 to 36 h prior to the arrival of dust aerosols over the EARLINET sites, so that each participating station can arrange the special measurements. The alerts are based on operational dust forecast of different regional models such as SKIRON (Kallos et al., 2006) and BSC-DREAM8b (Pérez et al., 2006a, b; Basart et al., 2012b). It is important to underline here, that the aim of this work is the quantitative comparison of BSC-DREAM8b capability to reproduce the desert dust vertical structure observed in a site of the Central Mediterranean region in terms of geometrical and optical properties of the dust layer. We do not want to analyse here in any way the model performance in terms of false positive and false negative dust cases forecast. The alerts are important for triggering the lidar measurements and collecting a large dataset of dust observations. Desert dust lidar measured profiles, which are completely independent on the BSC-DREAM8b model profiles, are used to quantitatively evaluate the BSC-DREAM8b model capability of reproducing the observed dust extinction vertical profile.

Therefore, only profiles affected by the desert dust particles are considered for evaluating the BSC-DREAM8b model capability of reproducing the desert dust particles arriving over Potenza. The identification of dust affected cases is performed following the same approach reported in Mona et al. (2006): (i) identifying layers in the free troposphere; (ii) checking potential desert origin by backtrajectories analysis and (iii) confirming the presence of dust outbreaks with satellite images/data. The experience gained within EARLINET in the observations/transport models integrated approach for the aerosol typing (Mattis et al., 2008; Mona et al., 2012b; Pappalardo et al.,

ACPD
13, 31363–31407, 2013

2013; Wandinger et al., 2011) allows a more precise identification of dust cases. In particular, the following steps forward were done respect to the Mona et al. (2006) climatological study on Saharan dust cases over Potenza: HYSPLIT 10-days backtrajectories analysis and FLEXPART model operated by the Norwegian Institute for Air Research (Stohl et al., 1998; Stohl and Thomson, 1999) were used for each layer using their flexibility in arrival time and altitude definition, different backtrajectories were used for doubtful situations, and finally we take advantage of the knowledge on dust intensive optical properties gained within EARLINET and for Potenza site in particular (Papayannis et al., 2008; Mona et al., 2006). The agreement with the 3 yr study of Mona et al. (2006) is really satisfying and around 93 %. Disagreement is related to cases with an integrated backscatter at 532 nm around 0.00023 sr^{-1} which is about 1 tenth of the observed mean values for the desert dust cases over Potenza reported by Mona et al. (2006).

A total number of 310 dust cases were selected for the analysis reported in the following. In particular, 58 and 248 aerosol extinction and backscatter coefficient profiles at 532 nm are considered, respectively. Additionally 352, 276 and 158 aerosol backscatter profiles at 355 and 1064 and aerosol extinction at 355 nm, respectively, were used for the evaluation of the dust layer geometrical properties discussed in Sect. 3.

2.2 The BSC-DREAM8b model

We used modeled extinction profiles from the BSC-DREAM8b model operated at the Barcelona Supercomputing Center – Centro Nacional de Supercomputación (BSC-CNS). BSC-DREAM8b provides operational forecasts since May 2009, and is also participating in the North Africa, Middle East and Europe (NA-ME-E) node of the SDS-WAS Programme. BSC-DREAM8b (Pérez et al., 2006a, b; Basart et al., 2012a) is a regional model designed to simulate and predict the atmospheric cycle of mineral dust aerosol. It solves the Euler-type partial differential non-linear equation for dust mass continuity and it is fully embedded as one of the governing prognosis equations in the atmospheric Eta/NCEP atmospheric model equations. The initial version of the

ACPD
13, 31363–31407, 2013

DREAM model (Nickovic et al., 2001) included the following features: (1) a dust uplifting scheme according to Shao et al. (1993), with addition of a viscous sub-layer approach between the surface and the lowest model layer (Janjic, 1994), (2) a simple wet-scavenging (Nickovic et al., 2001) and dry deposition (Giorgi, 1986) scheme, (3) horizontal and vertical advection, turbulent and lateral diffusion (Janjic, 1994), and (4) soil wetness effects on dust production (Fecan et al., 1999). The BSC-DREAM8b model (Pérez et al., 2006a, b), treats dust as a radiatively active substance with both short and long-wave outgoing radiation. Furthermore some other features are introduced, an updated dust production scheme based on the arid and semi-arid categories of the 1 km USGS land use dataset, a source size distribution derived from D'Almeida (1987), and in order to better couple the dust transport over long distances, a more detailed size bin distribution is used including eight size bins within 0.1–10 µm radius range according to Tegen and Lacis (1996).

The BSC-DREAM8b model has been evaluated for longer periods over North Africa and Europe (e.g., Jiménez-Guerrero et al., 2008; Basart et al., 2012a, b; Pay et al., 2010, 2012) and against experimental campaigns in source regions during the SAMUM-1 (Haustein et al., 2009, 2012) and the Bodélé Dust Experiments (BoDEx; Todd et al., 2008). Furthermore, daily evaluation of BSC-DREAM8b with near-real time observations is conducted in BSC-CNS. Currently, the daily operational model evaluation includes satellites (MODIS and MSG) and AERONET sun photometers. As far as the vertical distribution of aerosols some comparisons between lidar and forecast models profiles were performed for specific Saharan dust events in the Mediterranean Basin (e.g. Balis et al., 2004; Pérez et al., 2006a, b; Amiridis et al., 2009; Papanastasiou et al., 2010; Mona et al., 2012b).

ACPD
13, 31363–31407, 2013

Modeled AOD and dust extinction coefficient are related to column mass loading and mass concentration, respectively, by:

$$\tau(\lambda) = \sum_{k=1}^{8} \tau_k(\lambda) = \sum_{k=1}^{8} \frac{3}{4\rho_k r_k} M_k Q_{\text{ext}}(\lambda)_k$$

$$\alpha(\lambda) = \sum_{k=1}^{8} \alpha_k(\lambda) = \sum_{k=1}^{8} \frac{3}{4\rho_k r_k} C_k Q_{\text{ext}}(\lambda)_k$$

where for each size bin k: $\tau_k(\lambda)$ is the AOD, $\alpha_k(\lambda)$ the extinction coefficient, ρ_k is the particle mass density, r_k is the effective radius, M_k is the column mass loading, C_k is the concentration and $Q_{\text{ext}}(\lambda)_k$ is the extinction efficiency factor which was calculated using Mie scattering theory. For each size bin k and wavelength λ, the extinction efficiency was calculated with a Mie-algorithm based on the work of Mishchenko et al. (2002). Each particle is assumed to be homogeneous and spherical. Complex refractive indices are taken from the Global Aerosol Data Set (GADS) (Koepke et al., 1997).

The present analysis includes a dust simulation of BSC-DREAM8b for the period from 1 January 2000 to 31 December 2012 with hourly output. The initial state of dust concentration in the model was defined by the 24 h forecast from the previous-day model run. The NCEP final analyses (FNL; at $1^\circ \times 1^\circ$) at 00:00 UTC were used as initial conditions and boundary conditions at intervals of 6 h. The resolution was set to $1/3^\circ$ in the horizontal and to 24 layers extending up to approximately 15 km in the vertical. The domain of simulation covers northern Africa, Middle East and Europe.

3 Methodology

The 310 cases identified as Saharan dust cases observed over Potenza within the EARLINET database at its status on July 2013 are compared with the BSC-DREAM8b extinction vertical profiles (at 550 nm) through a quantitative methodology described in the following (flow chart reported in Fig. 1).

ACPD
13, 31363–31407, 2013

PEARL and BSC-DREAM8b profiles have different horizontal, vertical and temporal resolution. All these differences should be appropriately considered in our comparison. As concerns the horizontal resolution, PEARL data can be considered as point observations, while BSC-DREAM8b reports profiles on a uniform spatial grid of 0.3° × 0.3°. BSC-DREAM8b profiles are therefore averaged over points at a distance less than 15–30 km by PEARL lidar. Considering that over Potenza, the wind speed in the free troposphere is typically between 5–20 m s^{-1} (as resulting from ECMWF data), this would mean that we could expect a maximum shift in time of about 1.5 h. This temporal interval is comparable with the temporal resolution of both BSC-DREAM8b (1 h) and lidar (0.5–2.5 h) profiles used in this paper. This assures that comparable length scales are investigated.

BSC-DREAM8b provides profiles at fixed altitude ranges with resolution varying from 314 m (around 1.5 km altitude) up to 1461 m (around 15 km altitude). The PEARL lidar profiles have instead a typical effective vertical resolution of 60 m for the aerosol backscatter coefficient and ranging between 60 and 240 m for the aerosol extinction coefficient. The high vertical resolution of lidar makes indeed the lidar techniques the most powerful tool for investigating the vertical structure and composition of the atmosphere. In particular, aerosol optical properties profiles with high vertical resolution are very effective for aerosol layer/type identification and detection of the intrusion of long-range transported aerosol into PBL (e.g. Sakai et al., 2003; Mattis et al., 2008; Mona et al., 2012b; Pappalardo et al., 2013). In order to evaluate BSC-DREAM8b capability of reproducing dust vertical layering and dust optical properties, the original vertical resolution of lidar profiles was degraded to the resolution of the modeled profiles. Each lidar profile was then compared to the closest BSC-DREAM8b profile in time. However, BSC-DREAM8b are instantaneous profiles provided for each hour while measured lidar profiles are obtained integrating signals over a 0.5–2.5 h temporal window depending on the aerosol load (longer interval are needed for improving the signal-to-noise ratio in cases of smaller aerosol load). In addition, BSC-DREAM8b and lidar profiles are not simultaneous. For taking into account these temporal variances (different resolutions

ACPD
13, 31363–31407, 2013

and no-exact collocation), all comparisons have been performed for the each lidar profile also against the average of the BSC-DREAM8b hourly profiles in ±3 h around the central lidar time.

Besides desert dust, different aerosol types could coexist in the atmospheric column either at altitude ranges different from dust or mixed with dust particles. The analysis of air masses backtrajectories described in Sect. 1 was essential for identifying this kind of cases. During the period under investigation, we found about 10 dust cases with the presence of long-range transported aerosol different from desert particles at separated altitude ranges. These are cases of air masses coming from North America during forest fires and volcanic plume transported from Nabro, Eritrea (Sawamura et al., 2012). Even cirrus clouds can be observed simultaneously to desert dust but at different altitudes. For evaluating BSC-DREAM8b capability of reconstructing dust profiles over Central Mediterranean, the contribution of different aerosol sources to lidar profiles measured in Potenza was removed: i.e. the values of base and top of the dust layer were forced for each of the 10 cases to exclude altitude ranges with presence of other aerosol. After these layers are identified in lidar optical profile, the limitation in altitude range was performed manually on both the lidar and model profiles. The same procedure applies for cases in which cirrus clouds are detected in lidar observations.

Mixing with other kinds of aerosol could also occur. A typical example is the intrusion of Saharan dust into the local PBL, where local produced aerosol and pollution exists. Aerosol mixing situations are completely removed from this study. In particular, the comparison is carried out only in the free troposphere region, i.e. above the PBL as determined by lidar profiles (Matthias et al., 2004). This choice is related to the fact that the BSC-DREAM8b model forecasts only the dust contribution to the aerosol content but does not provide any information about local and/or different sources. Therefore all results reported in the following are related to altitude above the PBL top as identified in each single profile. The base of the dust layer was forced to be, also for model forecast, above the PBL top as determined by lidar measurements. Cases with mixing of dust and other sources in the free troposphere were not considered in the study. Finally,

ACPD
13, 31363–31407, 2013

cases of dust and volcanic particles, both mixed at the same level and separated in different vertical levels, collected for the Eyjafjallajökull eruption in 2010 (Mona et al., 2012b) are not considered here, because for those cases BSC-DREAM8b routinely data were used for investigating the effective origin of the particles, i.e. the dust identification in the measured profiles is not completely independent by the model outputs.

The aim of the paper is to evaluate the capability of BSC-DREAM8b to reproduce the desert dust as observed by lidar in a site of the Central Mediterranean region. The first step is the case-by-case identification of the altitude region affected by dust. Desert dust coming from Sahara can reach Potenza at different altitudes from the ground up to 9 km or more (Mona et al., 2006, 2007).

An algorithm was implemented for the quantitative identification of layers above the PBL. The main concept is that layer features can be identified through the gradient in the particle backscatter profile as reported in Mona et al. (2006, 2012b). In those papers the first maximum above the PBL of the first derivative of the aerosol profile was identified as base of the aerosol layer. We found that the application of this method to the lidar profiles degraded to the BSC-DREAM8b vertical resolution leads typically to an overestimation of the layer base respect to what obtained from the full resolution lidar profiles and in some cases to the impossibility to define a base layer. For overcoming these problems, the first point of positive gradient in the aerosol profile is used as indicator of the layer base as it indicates that the aerosol content increases after the natural decrease with the altitude toward the PBL top altitude.

The top of the desert dust layer from lidar profiles is identified as the first altitude point above the layer base where aerosol backscatter is higher than a fixed threshold and its derivative is null. It is assumed that within the dust layer the backscatter value is higher than the climatological mean evaluated in the 6.5–8.5 km altitude range, which is typically not affected by significant particle transport.

The determination of base/top from BSC-DREAM8b vertical profiles was done considering that these profiles provide information only for the desert dust particles: no-null values in the profiles correspond to altitude ranges affected by dust. An extinction value

ACPD
13, 31363–31407, 2013

$(1 \times 10^{-10}\,\mathrm{m}^{-1})$ is considered as minimum value for the layer identification, for taking into account the model uncertainty for low aerosol amount. The dust layer base from BSC-DREAM8b is calculated as the first point above the PBL (as estimated from lidar data) where the profile or its derivative increases, situations corresponding to an identifiable increase of optical properties out of the PBL respect to the typical decrease with the altitude of the aerosol optical.

The base and top altitude calculation is performed for each set of lidar simultaneous profiles (for example a complete dataset of 3 backscatter and 2 extinction profiles measured at the different wavelengths) on the backscatter profile at the longest available wavelength for taking advantage of the higher sensitivity to aerosol structures at longer wavelengths. If backscatter profiles are not available for a simultaneous lidar dataset, base and top of the dust layer are retrieved from the extinction profiles at the longest available wavelength. Once base and top are estimated for both lidar and model profiles, we estimate the center of mass of the dust layer as the mean altitude of the identified layer weighted by the altitude-dependent aerosol optical properties (Mona et al., 2006). Assuming the microphysical properties to be homogeneous within the aerosol layer, this quantity indicates the altitude where the most relevant part of the aerosol load is located.

Base, top and center of mass are independently determined for lidar and model profiles case by case. Geometrical features of dust layers as obtained by the 2 platforms are compared and discussed in Sect. 4. The linear correlation between lidar and BSC-DREAM8b profiles within the base/top altitude range is calculated as an additional measure of the model capability of reproducing the aerosol profile in terms of its shape. Finally, the base/top identification method reported above allows the evaluation of the aerosol extinction modeled profiles.

ACPD
13, 31363–31407, 2013

4 Results

4.1 Layering

The methodology reported in the previous section was applied to 310 dust cases observed over Potenza and reported as Saharan dust cases in the EARLINET database as its status on July 2013. The main results for dust layer geometrical properties are summarized in Table 1.

The base of the dust layer as estimated from BSC-DREAM8b profiles is in good agreement with lidar observations: the difference between these 2 independently estimated values is on average -0.2 ± 0.5 km, with differences below 0.2 km (0.4 km) for 63 % (84 %) of the cases. There are instead few cases (26 out of 309) for which the base estimated from modeled profiles is at least 1 km lower than the corresponding lidar measured value. This is related to the difficult separation of local PBL and lofted dust when an intrusion into the PBL also occurred. In fact, the lidar base is identified at a further gradient in the vertical profile above the PBL, while the base for the model profile is identified as the first positive value in the extinction profile above the PBL. For such cases, measured optical properties profiles for the total aerosol corresponding to these positive values above the PBL could not show a clear gradient and therefore these values could be not identified as part of a dust layer.

The distribution of the BSC-DREAM8b layer base values (Fig. 2a) shows a good agreement with lidar observations in terms of assumed values and distribution shape. The mean BSC-DREAM8b estimation for the dust base altitude is 2.3 ± 0.6 km and is in agreement within the errors with lidar measured mean value of 2.5 ± 0.7 km. The agreement is almost perfect for both the mean value and standard deviation that can be regarded as a measure of the variability of the dust layer base altitude. The high linear correlation coefficient (0.958) between the distributions reported in Fig. 2a is a quantitative measure of the observed agreement between observations and model in terms of layer base altitude.

ACPD
13, 31363–31407, 2013

Larger differences are observed for the top altitude of the dust layer for which the model overestimates 2.5 km on average. The distributions reported in Fig. 2b show that BSC-DREAM8b counts for many cases with top altitude up to 15 km, while lidar measurements observed dust above 10 km only in few cases. This gives a difference of 2 km in the mean value and an overestimation of its variability of more than 1 km for the model (see Table 1). The observed difference in top altitude reveals that dust particles are often present in the model at very high altitudes, while not observed in lidar profiles. The lidar top altitude identification is limited by the signal-to-noise ratio, and therefore lidar observations may underestimate the top altitude of the dust layer in some cases. However, the high occurrence of modeled top values above 15 km outlines model limitations at high altitudes. Additionally to some problems associated to the vertical diffusion in the model (Hong et al., 1996), another possible reason of this is that once dust achieves altitudes above the tropopause (> 12 km a.s.l.), the removal processes (i.e., wet and dry deposition) are less effective and as a consequence the time residence of dust is larger.

The comparison is significantly improved limiting the range of interest below 10 km (reported in Table 1 in bold face): an almost perfect agreement is found for mean values and standard deviation and the correlation coefficient between the two distributions increased from 0.802 to 0.932.

An interesting quantity for investigating aerosol layers is the layer Center of Mass (CoM hereafter). The dynamical behaviour (in time and altitude) of the whole layer can be described by the CoM evolution in absence of wind shear and under the assumption of homogeneity of aerosol microphysical properties within the layer. This would mean, for instance, that the origin of the dust particles and the travelled path could be investigated by the backtrajectory analysis of air masses arriving at the CoM altitude in the observational point. The altitude range around the CoM is also the region where most of the aerosol particles are located. This altitude is more representative of the whole aerosol layer than the altitude corresponding to the optical property peak value, because this latter could also correspond to an isolated extreme point. The CoM al-

ACPD
13, 31363–31407, 2013

titude as obtained from PEARL and BSC-DREAM8b profile assumes values between 1.5 and 9.5 km a.s.l., with mean value around 3.5 km and a variability (estimated as the standard deviation) of about 1 km. The BSC-DREAM8b model on average well reproduces the CoM of the identified dust layers with an almost perfect agreement with lidar measurements in terms of mean value, variability and distribution shape (see Table 1 and Fig. 2c). We found very good performance of the model also for the estimation of this quantity for each single case. Figure 3 reports the distribution of the difference between the CoM as measured by PEARL and that modeled by BSC-DREAM8b. 95 % of the values are between −2 and 2 km of difference. The model overestimates the CoM in more than 2 km for 7 cases and in only 2 cases the BSC-DREAM8b CoM is more than 2 km lower than lidar measured value. In particular, one −5 km difference occurs for the 21 August 2000 case: the base of the layer is around 3.9 km for both systems while the top is seen at about 10 km and 15 km for lidar and model respectively. Moreover the BSC-DREAM8b forecasted a layer extending from the base around 3.9 km with extinction significantly decreased at about 7 km and a further enhancement of it above 9 km with a peak at about 13 km. The corresponding PEARL profile shows no significant aerosol backscatter above 10 km. Although these sporadic (5 %) case, there is an almost perfect agreement on average, with a mean difference of -0.3 ± 1.0 km, comparable to the model vertical resolution in 1–2 km altitude range. The differences for the CoM are distributed according to a Gaussian curve (correlation coefficient of 0.986) centered at -0.17 ± 0.02 km with a standard deviation of 0.6 ± 0.02 km.

The linear correlation coefficient r_{prof} between aerosol lidar-measured optical properties and modeled extinction profiles (Fig. 4) is used as additional parameter for the description of the BSC-DREAM8b capability to reproduce the measured dust profiles. The correlation is calculated within the portion of profile extending between the base and the top of the dust layer as evaluated from the lidar profiles. This study has been performed comparing the modeled extinction vs the corresponding backscatter profile at 532 nm, as is the most abundant lidar product available during the 2000–2012 period. We found that in about 60 % of the cases, the 2 profiles are correlated within 5 %

ACPD
13, 31363–31407, 2013

of significance ($r_{prof} > 0.65$). Uncorrelated profiles are mainly related to cases of low aerosol load (see Fig. 5). 70 % of the cases with r_{prof} lower than 0.6 corresponds to an aerosol optical depth (BSC-DREAM8b estimated) lower than 0.1. Few outliers are visible in Fig. 5 with AOD in the 0.4–0.8 range and negative correlation coefficients: 16 April 2009, 18 May 2008 and 19 May 2008. From lidar measurements and data analysis, we found that these cases correspond to high variable situation, cloud formation at top of the dust layer and very sharp no-collocated decrease in both profiles, respectively.

The results reported above are obtained considering the BSC-DREAM8b profile closest in time to the lidar observation time. However the same analysis (not reported for shortness) has been carried out considering the average of BSC-DREAM8b profiles on 6 h around the lidar profile central time. Results for 6 h profiles are almost equal to those obtained for the closest in time modeled profiles, in terms of mean, standard deviation, correlation values and distributions for all the considered geometrical properties (base, top and center of mass of the layer) and for the linear correlation between the lidar and modeled profiles.

4.2 Optical properties

Aerosol extinction coefficient profiles at 532 nm as measured by PEARL lidar are available for 58 cases. The mean aerosol extinction profiles are calculated for lidar and model as average on these cases within the dust layer (Fig. 6). The PEARL extinction values at 532 nm are directly compared with the BSC-DREAM8b extinction at 550 nm, because of the short distance between these 2 wavelengths and because a small spectral extinction dependence is found for desert dust at this site (Boselli et al., 2012). We found a satisfying agreement for both the mean extinction profile and its standard deviations, i.e. its variability into the atmosphere over the considered cases. Aerosol extinction values are comparable as absolute number and, in agreement with results reported in Sect. 3.1, the shape of the profiles are similar above 3 km of altitude. It is interesting to note the larger bias between model and lidar in summer in comparison

ACPD
13, 31363–31407, 2013

with spring below 4 km of altitude. This could be partly associated to differences in the desert dust sources that affect Potenza along the annual cycle. Also, in summer, when the photochemical reactions are enhanced, higher extinction observed values at low levels could be associated to aged dust particles and the presence of other aerosols.

The distribution of the extinction values show that the BSC-DREAM8b model accounts for more low aerosol extinction values ($< 2\times10^{-5}$ m^{-1}) than lidar measurements (Fig. 7). About this point is important to underline that this comparison is performed on altitude ranges where both lidar and model values are available, i.e. where the aerosol load is such that we are above the lidar detection limit. The overestimation of the frequency of low extinction values could also be due to the presence within the dust layer of different particles within the lidar measured profiles and to difficulties in modeling optical properties modification/mixing processes occurred during the transport toward the measuring site. In this respect, it is worth mentioning that aged dust particles typically correspond to a longer travelled path, lower concentration numbers, and higher extinction efficiency of each particle. One source of uncertainty in BSC-DREAM8b is the consideration of desert dust aerosols as dry and inert. Therefore, the model does not consider this aging process. As a consequence, we would have lower modeled extinction coefficient values as combination of low concentration number and modeled extinction efficiency lower than the real one. Another possible reason of this overestimation could be associated to an overestimation of the fine fraction by the model (Pay et al., 2010; Basart et al., 2012b).

Removing extinction values lower than 2×10^{-5} m^{-1}, the linear correlation coefficient between the 2 distributions reported in Fig. 7 increases from 0.60, obtained considering all the values, to 0.86. This indicates that, apart from these values range, a good agreement is found in a climatological sense between the measured and modeled extinction values for dust.

The tendency to forecast low values of the extinction in the considered model is shown also in the scatter plot of all the forecast vs measured extinction values (Fig. 8a). There is not a linear correlation, neither a mathematical relationship, be-

ACPD
13, 31363–31407, 2013

tween the 2 datasets. Extinction values as modeled by BSC-DREAM8b are also compared to PEARL measurements of aerosol backscatter values within the dust layers (Fig. 8b), expanding the available couple of compared values. There is not a linear correlation between these 2 quantities. Mean values in backscatter interval range (red squares) show that modeled aerosol extinction is on average almost constant around $2.4 \times 10^{-5}\,m^{-1}$ for backscatter measured values lower than $3 \times 10^{-6}\,m^{-1}\,sr^{-1}$. In the 3 to $5 \times 10^{-6}\,m^{-1}\,sr^{-1}$ backscatter value range, BSC-DREAM8b forecasts extinction values comparable to the backscatter measured ones (extinction to backscatter ratio around 1 sr). Only 5 backscatter values higher than $5 \times 10^{-6}\,m^{-1}\,sr^{-1}$ were observed within the dust layer and correspond to an extinction to backscatter ratio around 10 sr against typical lidar ratio values at 532 nm around 40–60 sr for dust observed over Potenza (Mona et al., 2009).

Limiting the ratio values to 0–200 sr interval range (89 % of the cases), the mean ratio between the modeled extinction and measured backscatter inside the identified dust layer (35.9 sr) is in fair agreement with the Potenza Saharan dust lidar (extinction to backscatter) ratio measurements. This fair agreement is the result of the good agreement seen in the extinction profiles in Fig. 6. However Fig. 8 shows that the case-by-case comparison is not satisfying. In addition, the extinction (modeled) to backscatter (measured) ratio is distributed according to a log-normal distribution, against the experimental evidence of a Gaussian type distribution for this intensive property for dust particles at this site (Mona et al., 2006). A log-normal distribution, on the contrary, has been observed as typical for extensive (number concentration dependent) properties like aerosol extinction and backscatter (e.g. Matthias et al., 2004). This extinction vs backscatter comparison is a further confirmation that the dust mixing/modification processes are significant in this region of the Mediterranean.

ACPD
13, 31363–31407, 2013

5 Summary and conclusions

The database of dust optical properties profiles collected at Potenza, Southern Italy since 2000 by a multi-wavelength Raman lidar has been used to evaluate the BSC-DREAM8b capability to reproduce dust profiles in terms of dust layer geometrical and optical properties. This is to our knowledge the first systematic and quantitative evaluation of dust modeled profiles through Raman lidar measurements.

A suitable methodology for taking into account different resolutions (in horizontal, vertical and temporal domains) and external aerosol mixing situations has been identified. The comparison methodology has been developed paying particular attention to its potential further applications to other sites (in particular EARLINET stations) and models. The BSC-DREAM8b model well reconstructs on average the observed profiles, even if with some exceptions.

The base of the dust layer is found to be around 2.5 km a.s.l. and is in agreement with observations, but it should be considered that we limited our comparison above the local PBL, forcing in some way this agreement. An observed tendency of the BSC-DREAM8b model to overestimate the dust layer top height, with values of about 15 km in 32 % of the cases could be related to a too long aerosol life time in the model scheme resulting from little removal of aerosol. The top altitude of the dust layer is furthermore a parameter not suitable for the extension of this study to other stations/networks because the sensitivity of lidar is a characteristic of each one instrument and therefore the comparison in terms of the top altitude would have no meaning at network level. We found that the center of mass of the dust layer is the best suitable geometrical parameter for evaluating the capability of the dust model to capture the dust plume in the vertical dimension. The BSC-DREAM8b model CoM is consistent with a high confidence level (correlation coefficient 0.986) with respect to lidar measurements. In particular case-by-case difference is on average 0.3 ± 1.0 km. The shape of the lidar profile is also well reconstructed by BSC-DREAM8b (within 5 % of significance) for

ACPD
13, 31363–31407, 2013

60 % of the cases. Uncorrelated profiles are related in 70 % of the cases to AOD lower than 0.1.

The extinction coefficient as modelled by BSC-DREAM8b underestimates measured values in particular at altitude lower than 3.5 km probably because the model does not consider aerosol internal mixing and modification processes, producing an unrealistic high occurrence of values less than $2 \times 10^{-5}\,m^{-1}$. Observation vs model scatter plots and the resulting lidar ratio values show that BSC-DREAM8b could be furthermore improved for the extinction coefficient value forecast, in particular in the low altitude ranges. Further relevant differences are observed for low concentrations, where however lidar and model uncertainty are not negligible. The large database of high quality Saharan dust observations provided by EARLINET (Papayannis et al., 2008) is the best candidate for a systematic comparison with dust model outputs aiming at the evaluation of dust models performances over the European continent, that is, over a large area characterized by different aerosol content regions (Mediterranean, continental Europe, Northern Europe, and Eastern-polluted countries).

The study reported in this paper can be considered as a pilot case in which we developed a specific methodology to be applied to the whole EARLINET network and to other models in the framework of the SDS-WAS program. Particular valuable for enlarging the evaluation to all EARLINET station is the infrastructural improvement planned within ACTRIS for the provision of aerosol layering as further standard EARLINET product.

For the extinction coefficient improvement, it would be important having information about microphysical aerosol properties. In this sense, novel inversion codes able to provide profiles of microphysical properties by collocated lidar and sun-photometer data for example could provide the missing information for an appropriate parameterization (Wagner et al., 2013). Moreover, concentration-to-extinction conversion factor dependence on intensive properties like lidar ratio and depolarization ratio could be investigated through specific measurement campaigns, as the ACTRIS summer 2012–

ACPD
13, 31363–31407, 2013

2013 campaigns with intensive measurements performed at EARLINET and ACTRIS in situ sites in conjunction with EMEP and Charmex campaigns.

Acknowledgements. The financial support for EARLINET by the European Union under grant RICA 025991 in the Sixth Framework Programme is gratefully acknowledged. Since 2011 EARLINET has been integrated in the ACTRIS Research Infrastructure Project supported by the European Union Seventh Framework Programme (FP7/2007–2013) under grant agreement no. 262254. J. M. Baldasano and S. Basart acknowledge the "Supercomputación and e-ciencia" Project (CSD2007-0050) from the Consolider-Ingenio 2010 program and Severo Ochoa (SEV-2011-00067) program of the Spanish Goverment. BSC-DREAM8b simulations were performed on the Mare Nostrum supercomputer hosted by Barcelona Supercomputing Center-Centro Nacional de Supercomputación (BSC-CNS). Authors would like to thank the NOAA Air Resources Laboratory (ARL) for the provision of the HYSPLIT backtrajectory analysis and the Norwegian Institute for Air Research for the FLEXPART model. The work performed by M. G. Cava during her bachelor degree thesis is greatly acknowledged. The authors would like to thank C. Pérez (Department of Applied Physics and Applied Math, Columbia University, New York, USA) for comments on the manuscript.

References

Alfaro, S. C., Lafon, S., Rajot, J. L., Formenti, P., Gaudichet, A., and Maille, M.: Iron oxides and light absorption by pure desert dust: an experimental study, J. Geophys. Res.-Atmos., 109, D08208, doi:10.1029/2003JD004374, 2004.

Amiridis, V., Kafatos, M., Pérez, C., Kazadzis, S., Gerasopoulos, E., Mamouri, R. E., Papayannis, A., Kokkalis, P., Giannakaki, E., Basart, S., Daglis, I., and Zerefos, C.: The potential of the synergistic use of passive and active remote sensing measurements for the validation of a regional dust model, Ann. Geophys., 27, 3155–3164, doi:10.5194/angeo-27-3155-2009, 2009.

Amiridis, V., Wandinger, U., Marinou, E., Giannakaki, E., Tsekeri, A., Basart, S., Kazadzis, S., Gkikas, A., Taylor, M., Baldasano, J., and Ansmann, A.: Optimizing Saharan dust CALIPSO retrievals, Atmos. Chem. Phys. Discuss., 13, 14749–14795, doi:10.5194/acpd-13-14749-2013, 2013.

ACPD
13, 31363–31407, 2013

Ansmann, A., Riebesell, M., Wandinger, U., Weitkamp, C., Voss, E., Lahmann, W., and Michaelis, W.: Combined Raman elastic-backscatter lidar for vertical profiling of moisture, aerosol extinction, backscatter and lidar ratio, Appl. Phys. B., 55, 18–28, 1992.

Ansmann, A., Bösenberg, J., Chaikovsky, A., Comerón, A., Eckhardt, S., Eixmann, R., Freudenthaler, V., Ginoux, P., Komguem, L., Linné, H., Márquez, M. A. L., Matthias, V., Mattis, I., Mitev, V., Müller, D., Music, S., Nickovic, S., Pelon, J., Sauvage, L., Sobolewsky, P., Srivastava, M. K., Stohl, A., Torres, O., Vaughan, G., Wandinger, U., and Wiegner, M.: Long-range transport of Saharan dust to northern Europe: the 11–16 October 2001 outbreak observed with EARLINET, J. Geophys. Res., 108, 4783, doi:10.1029/2003JD003757, 2003.

Ansmann, A., Tesche, M., Groß, S., Freudenthaler, V., Seifert, P., Hiebsch, A., Schmidt, J., Wandinger, U., Mattis, I., Müller, D., and Wiegner, M.: The 16 April 2010 major volcanic ash plume over central Europe: EARLINET lidar and AERONET photometer observations at Leipzig and Munich, Germany, Geophys. Res. Lett., 37, L13810, doi:10.1029/2010GL043809, 2010.

Balis, D. S., Amiridis, V., Nickovic, S., Papayannis, A., and Zerefos, C.: Optical properties of Saharan dust layers as detected by a Raman lidar at Thessaloniki, Greece, Geophys. Res. Lett., 31, L13104, doi:10.1029/2004GL019881, 2004.

Basart, S., Pérez, C., Nickovic, S., Cuevas, E., Schulz, M., and Baldasano, J. M.: Development and evaluation of BSC-DREAM8b dust regional model over Northern Africa, the Mediterranean and the Middle East regions, Tellus B, 64, 18539, doi:10.3402/tellusb.v64i0.18539, 2012a.
b !

Basart, S., Pay, M. T., Jorba, O., Pérez, C., Jiménez-Guerrero, P., Schulz, M., and Baldasano, J. M.: Aerosols in the CALIOPE air quality modelling system: evaluation and analysis of PM levels, optical depths and chemical composition over Europe, Atmos. Chem. Phys., 12, 3363–3392, doi:10.5194/acp-12-3363-2012, 2012b.

Böckmann, C., Wandinger, U., Ansmann, A., Bösenberg, J., Amiridis, V., Boselli, A., Delaval, A., De Tomasi, F., Frioud, M., Grigorov, I., Hågård, A., Horvat, M., Iarlori, M., Komguem, L., Kreipl, S., Larchevêque, G., Matthias, V., Papayannis, A., Pappalardo, G., Rocadenbosch, F., Rodrigues, J. A., Schneider, J., Shcherbakov, V., and Wiegner, M.: Aerosol lidar intercomparison in the framework of the EARLINET project. 2. Aerosol backscatter algorithms, Appl. Optics, 43, 977–989, 2004.

ACPD
13, 31363–31407, 2013

Böckmann, C., I., Mironova, I., Müller, D., Scheidenbach, L., and Nessler, R.: Microphysical aerosol parameters from multiwavelength lidar, J. Opt. Soc. Am. A, 22, 518–528, 2005.

Bösenberg, Matthias, J. V., Matthias, V., Amodeo, A., Amoiridis, V., Ansmann, A., Baldasano, J. M., Balin, I., Balis, D., Böckmann, C., Boselli, A., Carlsson, G., Chaikovsky, A., Chourdakis, G., Comerón, A., De Tomasi, F., Eixmann, R., Freudenthaler, V., Giehl, H., Grigorov, I., Hågård, A., Iarlori, M., Kirsche, A., Kolarov, G., Komguem, L., Kreipl, S., Kumpf, W., Larchevêque, G., Linné, H., Matthey, R., Mattis, I., Mekler, A., Mironova, I., Mitev, V., Mona, L., Müller, D., Music, S., Nickovic, S., Pandolfi, M., Papayannis, A., Pappalardo, G., Pelon, J., Pérez, C., Perrone, R. M., Persson, R., Resendes, D. P., Rizi, V., Rocadenbosch, F., Rodrigues, A., Sauvage, L., Schneidenbach, L., Schumacher, R., Shcherbakov, V., Simeonov, V., Sobolewski, P., Spinelli, N., Stachlewska, I., Stoyanov, D., Trickl, T., Tsaknakis, G., Vaughan, G., Wandinger, U., Wang, X., Wiegner, M., Zavrtanik, M., and Zerefos, C.: EARLINET: a European Aerosol Research Lidar Network to Establish an Aerosol Climatology, Max-Planck-Institut Report No. 348, Hamburg, Germany, 2003.

Boselli, A., Caggiano, R., Cornacchia, C., Madonna, F., Macchiato, M., Mona, L., Pappalardo, G., and Trippetta, S.: Multi year sun-photometer measurements for aerosol characterization in a Central Mediterranean site, Atmos. Res., 104, 98–110, doi:10.1016/j.atmosres.2011.08.002, 2012.

Carslaw, K. S., Boucher, O., Spracklen, D. V., Mann, G. W., Rae, J. G. L., Woodward, S., and Kulmala, M.: A review of natural aerosol interactions and feedbacks within the Earth system, Atmos. Chem. Phys., 10, 1701–1737, doi:10.5194/acp-10-1701-2010, 2010.

D'Almeida, G. A.: Desert aerosol characteristics and effects on climate, in: Palaeoclimatology and Palaeometeorology: Modern and Past Patterns of Global Atmospheric Transport, edited by: Leinen, M. and Sarnthein, M., NATO ASI Series, C, vol. 282, 311–338, 1987.

De Longueville, F., Hountondji, Y.-C., Henry, S., and Ozer, P.: What do we know about effects of desert dust on air quality and human health in West Africa compared to other regions?, Sci. Total. Environ., 409, 1–8, doi:10.1016/j.scitotenv.2010.09.025, 2013.

Escudero, M., Querol, X., Ávila, A., and Cuevas, E.: Origin of the exceedances of the European daily PM limit value in regional background areas of Spain, Atmos. Environ., 41, 730–744, 2007.

European Comission: Commission Staff Working Paper establishing guidelines for demonstration and subtraction of exceedances attributable to natural sources under the Directive 2008/50/EC on ambient air quality and cleaner air for Europe, 2011.

ACPD
13, 31363–31407, 2013

Fécan, F., Marticorena, B., and Bergametti, G.: Parametrization of the increase of the aeolian erosion threshold wind friction velocity due to soil moisture for arid and semi-arid areas, Ann. Geophys., 17, 149–157, doi:10.1007/s00585-999-0149-7, 1999.

Ferrare, R. A., Melfi, S. H., Whiteman, D. N., Evans, K. D., Poellot, M., and Kaufman, Y. J.: Raman lidar measurements of aerosol extinction and backscattering: 2. Derivation of aerosol real refractive index, single-scattering albedo, and humidification factor using Raman lidar and aircraft size distribution measurements, J. Geophys. Res., 103, (D16), 19673–19689, doi:10.1029/98JD01647, 1998.

Ferrare, R. A., Turner, D. D., Brasseur, L. H., Feltz, W. F., Dubovik, O., and Tooman, T. P.: Raman lidar measurements of the aerosol extinction-to-backscatter ratio over the Southern Great Plains, J. Geophys. Res., 106, (D17), 20333–20347, doi:10.1029/2000JD000144, 2001.

Ferrare, R. A., Browell, E. V., Hair, J. W., Ismail, S., Turner, D. D., Clayton, M., Butler, C., Brackett, V. G., Fenn, M. A., Notari, A., Kooi, S. A., Chin, M., Guibert, S., Schulz, M., Chuang, C., Krol, M., Bauer, S. E., Liu, X., Myhre, G., Seland, Ø., Fillmore, D., Ghan, S., Gong, S., Ginoux, P., and Takemura, T.: The vertical distribution of aerosols: lidar measurements vs. model simulations, in: Reviewed and revised papers presented at the 23rd International Laser Radar Conference, Nara Japan, 24–28 July 2006, Chikao Nagasawa and Nobuo Sugimoto Editors, 2006.

Ford, B. and Heald, C. L.: An A-train and model perspective on the vertical distribution of aerosols and CO in the Northern Hemisphere, J. Geophys. Res., 117, D06211, doi:10.1029/2011JD016977, 2012.

Franzen, L. G., Hjelmroos, M., Kallberg, P., Brorstrom-Lunden, E., Juntto, S., and Savolainen, A. L.: The "yellow snow" episode of northern Fennoscandia, March 1991 – a case study of long-distance transport soil, pollen and stable organic compounds, Atmos. Environ., 28, 3587–3604, 1994.

Freudenthaler, V., Esselborn, M., Wiegner, M., Heese, B., Tesxhe, M., Ansmann, A., Müller, D., Althausen, D., Wirth, M., Fix, A., Ehret, G., Knippertz, P., Toledano, C., Gasteiger, J., Garhammer, M., and Seefeldner, M.: Depolarization ratio profiling at several wavelengths in pure Saharan dust during SAMUM 2006, Tellus B, 61, 165–179, doi:10.1111/j.1600-0889.2008.00396.x, 2009.

Gallisai, R., Peters, F., Basart, S., and Baldasano, J. M.: Mediterranean basin-wide correlations between Saharan dust deposition and ocean chlorophyll concentration, Biogeosciences Discuss., 9, 8611–8639, doi:10.5194/bgd-9-8611-2012, 2012.

ACPD
13, 31363–31407, 2013

Generoso, S., Bey, I., Labonne, M., and Bréon, F.-M.: Aerosol vertical distribution in dust outflow over the Atlantic: comparisons between GEOS-Chem and Cloud-Aerosol Lidar and Infrared Pathfinder Satellite Observation (CALIPSO), J. Geophys. Res., 113, D24209, doi:10.1029/2008JD010154, 2008.

Giorgi, F.: A particle dry7deposition parameterization scheme for use in tracer transport models, J. Geophys. Res., 91, 9794–9806, 1986.

Gobbi, G. P., Barnaba, F., Ammannato, L.: Estimating the impact of Saharan dust on the year 2001 PM_{10} record of Rome, Atmos. Environ., 41, 261–275, doi:10.1016/j.atmosenv.2006.08.036, 2007.

xxx !!!

Gobbi, G. P., Angelini, F., Barnaba, F., Costabile, F., Baldasano, J. M., Basart, S., Sozzi, R., and Bolignano, A.: Changes in particulate matter physical properties during Saharan advections over Rome (Italy): a four-year study, 2001–2004, Atmos. Chem. Phys., 13, 7395–7404, doi:10.5194/acp-13-7395-2013, 2013.

Hara, Y., Yumimoto, K., Uno, I., Shimizu, A., Sugimoto, N., Liu, Z., and Winker, D. M.: Asian dust outflow in the PBL and free atmosphere retrieved by NASA CALIPSO and an assimilated dust transport model, Atmos. Chem. Phys., 9, 1227–1239, doi:10.5194/acp-9-1227-2009, 2009.

Hart, W. D., Spinhirne, J. D., Palm, S. P., and Hlavka, D. L.: Height distribution between cloud and aerosol layers from the GLAS spaceborne lidar in the Indian Ocean region, Geophys. Res. Lett., 32, L22S06, doi:10.1029/2005GL023671, 2005.

Haustein, K., Pérez, C., Baldasano, J. M., Müller, D., Tesche, M., Schladitz, A., Freudenthaler, V., Heese, B., Esselborn, M., Weinzierl, B., Kandler, K., and von Hoyningen-Huene, W.: Regional dust model performance during SAMUM 2006, Geophys. Res. Lett., 36, L03812, doi:10.1029/2008GL036463, 2009.

Haustein, K., Pérez, C., Baldasano, J. M., Jorba, O., Basart, S., Miller, R. L., Janjic, Z., Black, T., Nickovic, S., Todd, M. C., Washington, R., Müller, D., Tesche, M., Weinzierl, B., Esselborn, M., and Schladitz, A.: Atmospheric dust modeling from meso to global scales with the online NMMB/BSC-Dust model – Part 2: Experimental campaigns in Northern Africa, Atmos. Chem. Phys., 12, 2933–2958, doi:10.5194/acp-12-2933-2012, 2012.

Henriksson, A. S., Sarnthein, M., Eglinton, G., and Poynter, J.: Dimethylsulfide production variations over the past 200 k.y. in the equatorial Atlantic: a first estimate, Geology, 28, 499–502, doi:10.1130/0091-7613(2000)28<499:DPVOTP>2.0.CO;2, 2000.

ACPD
13, 31363–31407, 2013

Hong, S.-Y., and Pan, H.-L.: Nonlocal boundary layer vertical diffusion in a medium-range forecast model, Mon. Weather Rev., 124, 2322–2339, 1996.

Janjic, Z. I.: The step-mountain eta coordinate model: further developments of the convection, viscous sublayer and turbulence closure schemes, Mon. Weather Rev., 122, 927–945, 1994.

Jiménez-Guerrero, P., Pérez, C., Jorba, O., and Baldasano, J. M.: Contribution of Saharan dust in an integrated air quality system and its on-line assessment, Geophys. Res. Lett., 35, L03814, doi:10.1029/2007GL031580, 2008.

Kallos, G., Papadopoulos, A., Katsafados, P., and Nickovic, S.: Transatlantic Saharan dust transport: model simulation and results, J. Geophys. Res., 111, D09204, doi:10.1029/2005JD006207, 2006.

Kinne, S., Schulz, M., Textor, C., Guibert, S., Balkanski, Y., Bauer, S. E., Berntsen, T., Berglen, T. F., Boucher, O., Chin, M., Collins, W., Dentener, F., Diehl, T., Easter, R., Feichter, J., Fillmore, D., Ghan, S., Ginoux, P., Gong, S., Grini, A., Hendricks, J., Herzog, M., Horowitz, L., Isaksen, I., Iversen, T., Kirkevåg, A., Kloster, S., Koch, D., Kristjansson, J. E., Krol, M., Lauer, A., Lamarque, J. F., Lesins, G., Liu, X., Lohmann, U., Montanaro, V., Myhre, G., Penner, J., Pitari, G., Reddy, S., Seland, O., Stier, P., Takemura, T., and Tie, X.: An AeroCom initial assessment – optical properties in aerosol component modules of global models, Atmos. Chem. Phys., 6, 1815–1834, doi:10.5194/acp-6-1815-2006, 2006.

Klein, H., Nickovic, S., Haunold, W., Bundke, U., Nillius, B., Ebert, M., Weinbruch, S., Schuetz, L., Levin, Z., Barrie, L. A., and Bingemer, H.: Saharan dust and ice nuclei over Central Europe, Atmos. Chem. Phys., 10, 10211–10221, doi:10.5194/acp-10-10211-2010, 2010.

Koepke, P., Hess, M., Schult, I., and Shettle, E. P.: Global aerosol dataset, Report N 243, Max-Plank-Institut für Meteorologie, Hamburg, 44 pp., September 1997.

Koffi, B., Schulz, M., Bréon, F.-M., Griesfeller, I., Winker, D., Balkanski, Y., Bauer, S., Berntsen, T., Chin, M., Collins, W. D., Dentener, F., Diehl, T., Easter, R., Ghan, S., Ginoux, P., Gong, S., Horowitz, L. W., Iversen, T., Kirkevåg, A., Koch, D., Krol, M., Myhre, G., Stier, P., and Takemura, T.: Application of the CALIOP layer product to evaluate the vertical distribution of aerosols estimated by global models: AeroCom phase I results, J. Geophys. Res., 117, D10201, doi:10.1029/2011JD016858, 2012.

Kwon, H. J., Cho, S. H., Chun, Y., Lagarde, F., and Pershagen, G.: Effects of the Asian dust events on daily mortality in Seoul, Korea, Environ. Res., 90, 1–5, 2002.

ACPD
13, 31363–31407, 2013

Liu, Z., Omar, A., Vaughan, M., Hair, J., Kittaka, C., Hu, Y. X., Powell, K., Trepte, C., Winker, D., Hostetler, C., Ferrare, R., and Pierce, R.: CALIPSO lidar observations of the optical properties of Saharan dust: a case study of long-range transport, J. Geophys. Res., 113, D07207, doi:10.1029/2007JD008878, 2008.

Madonna, F., Amodeo, A., Boselli, A., Cornacchia, C., Cuomo, V., D'Amico, G., Giunta, A., Mona, L., and Pappalardo, G.: CIAO: the CNR-IMAA advanced observatory for atmospheric research, Atmos. Meas. Tech., 4, 1191–1208, doi:10.5194/amt-4-1191-2011, 2011.

Matthias, V., Balis, D., Bösenberg, J., Eixmann, R., Iarlori, M., Komguem, L., Mattis, I., Papayannis, A., Pappalardo, G., Perrone, M. R., and and Wang, X.: The vertical aerosol distribution over Europe: statistical analysis of Raman lidar data from 10 EARLINET stations, J. Geophys. Res., 109, D18201, doi:10.1029/2004JD004638, 2004.

Mattis, I., Mueller, D., Ansmann, A., Wandinger, U., Preissler, J., Seifert, P., and Tesche, M.: Ten years of multiwavelength Raman lidar observations of free-tropospheric aerosol layers over central Europe: geometrical properties and annual cycle, J. Geophys. Res., 113, D20202, doi:10.1029/2007JD009636, 2008.

McGill, M. J., Li, L., Hart, W. D., Heymsfield, G. M., Hlavka, D. L., Racette, P. E., Tian, L., Vaughan, M. A., and Winker, D. M.: Combined lidar-radar remote sensing: initial results from CRYSTAL-FACE, J. Geophys. Res., 109, D07203, doi:10.1029/2003JD004030, 2004.

Mills, M. M., Ridame, C., Davey, M., La Roche, J., and Geider, R. J.: Iron and phosphorus co-limit nitrogen fixation in the eastern tropical North Atlantic, Nature, 429, 292–294, 2004.

Mishchenko, M. I., Travis, L. D., and Lacis, A. A.: Scattering, Absorption, and Emission of Light by Small Particles, Cambridge University Press, Cambridge UK, 2002.

Mishra, S. K. and Tripathi, S. N.: Modeling optical properties of mineral dust over the Indian Desert, J. Geophys. Res., 113, D23201, doi:10.1029/2008JD010048, 2008.

Mona, L., Amodeo, A., Pandolfi, M., and Pappalardo, G.: Saharan dust intrusions in the Mediterranean area: three years of Raman lidar measurements, J. Geophys. Res., 111, D16203, doi:10.1029/2005JD006569, 2006.

Mona, L., Amodeo, A., D'Amico, G., and Pappalardo, G.: First comparisons between CNR-IMAA multi-wavelength Raman lidar measurements and CALIPSO measurements, in: LIDAR technologies, techniques, and measurements for atmospheric remote sensing III, edited by: Upendra, N., and Singh, Pappalardo, G., P. SPIE, 6750, 675010, doi:10.1117/12.738011, 2007.

ACPD
13, 31363–31407, 2013

Mona, L., Pappalardo, G., Amodeo, A., D'Amico, G., Madonna, F., Boselli, A., Giunta, A., Russo, F., and Cuomo, V.: One year of CNR-IMAA multi-wavelength Raman lidar measurements in coincidence with CALIPSO overpasses: Level 1 products comparison, Atmos. Chem. Phys., 9, 7213–7228, doi:10.5194/acp-9-7213-2009, 2009.

Mona, L., Liu, Z., Mueller, D., Omar, A., Papayannis, A., Pappalardo, G., Sugimoto, N., and Vaughan, M.: Lidar measurements for desert dust characterization: an overview, Advances in Meteorology, 2012, 356265, doi:10.1155/2012/356265, 2012a.
b !

Mona, L., Amodeo, A., D'Amico, G., Giunta, A., Madonna, F., and Pappalardo, G.: Multi-wavelength Raman lidar observations of the Eyjafjallajökull volcanic cloud over Potenza, southern Italy, Atmos. Chem. Phys., 12, 2229–2244, doi:10.5194/acp-12-2229-2012, 2012b.

Müller, D., Franke, K., Ansmann, A., Althausen, D., and Wagner, F.: Indo-Asian pollution during INDOEX: microphysical particle properties and single-scattering albedo inferred from multiwavelength lidar observations, J. Geophys. Res., 108, 4600, doi:10.1029/2003JD003538, 2003.

Müller, D., Mattis, I., Ansmann, A., Wehner, B., Althausen, D., Wandinger, U., and Dubovik, O.: Closure study on optical and microphysical properties of an urban/arctic haze plume observed with Raman lidar and Sun photometer, J. Geophys. Res., 109, D13206, doi:10.1029/2003JD004200, 2004.

Müller, D., Ansmann, A., Mattis, I., Tesche, M., Wandinger, U., Althausen, D., and Pisani, G.: Aerosol-type-dependent lidar ratio observed with Raman lidar, J. Geophys. Res., 112, D16202, doi:10.1029/2006JD008292, 2007.

Müller, D., Heinold, B., Tesche, M., Tegen, I., Althausen, D., Alados Arboledas, L., Amiridis, V., Amodeo, A., Ansmann, A., Balis, D., Comeron, A., D'Amico, G., Gerasopoulos, E., Guerrero-Rascado, J. L., Freudenthaler, V., Giannakaki, E., Heese, B., Iarlori, M., Knippertz, P., Mamouri, R. E., Mona, L., Papayannis, A., Pappalardo, G., Perrone, R.-M., Pisani, G., Rizi, V., Sicard, M., Spinelli, N., Tafuro, A., and Wiegner, M.: EARLINET observations of the 14–22-May long-range dust transport event during SAMUM 2006: validation of results from dust transport modelling, Tellus B, 61, 325–339, 2009.

Nickovic, S., Kallos, G., Papadopoulos, A., and Kakaliagou, O.: A model for prediction of desert dust cycle in the atmosphere, J. Geophys. Res., 106, 18113–18130, doi:10.1029/2000JD900794, 2001.

ACPD
13, 31363–31407, 2013

Osterloh, L., Pérez, C., Böhme, D., Baldasano, J. M., Böckmann, C., Schneidenbach, L., and Vicente, D.: Software for the retrieval of aerosol microphysical properties from lidar data in the framework of EARLINET-ASOS, Comput. Phys. Commun., 180, 2095–2102, doi:10.1016/j.cpc.2009.06.011, 2009.

Papayannis, A., Amiridis, V., Mona, L., Tsaknakis, G., Balis, Bösenberg J., Chaikovski, A., De Tomasi, F., Grigorov, I., Mattis, I., Mitev, V., Müller D., Nickovic, S., Pérez C., Pietruczuk, A., Pisani, G., Ravetta, F., Rizi, V., Sicard, M., Trickl, T., Wiegner, M., Gerding, M., D'Amico, G., and Pappalardo, G.: Systematic lidar observations of aerosol optical properties during Saharan dust intrusions over Europe, in the frame of EARLINET (2000–2002): statistical analysis and results, J. Geophys. Res., 113, D10204, doi:10.1029/2007JD009028, 2008.

Pappalardo, G., Wandinger, U., Mona, L., Hiebsch, A., Mattis, I., Amodeo, A., Ansmann, A., Seifert, P., Linné, H., Apituley, A., Alados Arboledas, L., Balis, D., Chaikovsky, A., D'Amico, G., De Tomasi, F., Freudenthaler, V., Giannakaki, E., Giunta, A., Grigorov, I., Iarlori, M., Madonna, F., Mamouri, R.-E., Nasti, L., Papayannis, A., Pietruczuk, A., Pujadas, M., Rizi, V., Rocadenbosch, F., Russo, F., Schnell, F., Spinelli, N., Wang, X., and Wiegner, M.: EARLINET correlative measurements for CALIPSO: first intercomparison results, J. Geophys. Res., 115, D00H19, doi:10.1029/2009JD012147, 2010.

Pappalardo, G., Mona, L., D'Amico, G., Wandinger, U., Adam, M., Amodeo, A., Ansmann, A., Apituley, A., Alados Arboledas, L., Balis, D., Boselli, A., Bravo-Aranda, J. A., Chaikovsky, A., Comeron, A., Cuesta, J., De Tomasi, F., Freudenthaler, V., Gausa, M., Giannakaki, E., Giehl, H., Giunta, A., Grigorov, I., Groß, S., Haeffelin, M., Hiebsch, A., Iarlori, M., Lange, D., Linné, H., Madonna, F., Mattis, I., Mamouri, R.-E., McAuliffe, M. A. P., Mitev, V., Molero, F., Navas-Guzman, F., Nicolae, D., Papayannis, A., Perrone, M. R., Pietras, C., Pietruczuk, A., Pisani, G., Preißler, J., Pujadas, M., Rizi, V., Ruth, A. A., Schmidt, J., Schnell, F., Seifert, P., Serikov, I., Sicard, M., Simeonov, V., Spinelli, N., Stebel, K., Tesche, M., Trickl, T., Wang, X., Wagner, F., Wiegner, M., and Wilson, K. M.: Four-dimensional distribution of the 2010 Eyjafjallajökull volcanic cloud over Europe observed by EARLINET, Atmos. Chem. Phys., 13, 4429–4450, doi:10.5194/acp-13-4429-2013, 2013.

Pay, M. T., Piot, M., Jorba, O., Gassó, S., Gonçalves, M., Basart, S., Dabdub, D., Jiménez-Guerrero, P., and Baldasano, J. M.: A full year evaluation of the CALIOPE-EU air quality modeling system over Europe for 2004, Atmos. Environ., 44, 3322–3342, doi:10.1016/j.atmosenv.2010.05.040, 2010.

ACPD
13, 31363–31407, 2013

Pay, M. T., Jiménez-Guerrero, P., Jorba, O., Basart, S., Querol, X., Pandolfi, M., and Baldasano, J. M.: Spatio-temporal variability of concentrations and speciation of particulate matter across Spain in the CALIOPE modeling system, Atmos. Environ., 46, 376–396, 2012.

Pederzoli, A., Mircea, M., Finardi, S., di Sarra, A., and Zanini, G.: Quantification of Saharan dust contribution to PM_{10} concentrations over Italy during 2003–2005, Atmos. Environ., 44, 4181–4190, doi:10.1016/j.atmosenv.2010.07.031, 2010.

Pérez, C., Nickovic, S., Baldasano, J. M., Sicard, M., Rocadenbosch, F., and Cachorro, V. E.: A long Saharan dust event over the western Mediterranean: lidar, sun photometer observations, and regional dust modeling, J. Geophys. Res., 111, D15214, doi:10.1029/2005JD006579, 2006a.

Pérez, C., Nickovic, S., Pejanovic, G., Baldasano, J. M., and Ozsoy, E.: Interactive dust-radiation modeling: a step to improve weather forecasts, J. Geophys. Res., 11, D16206, doi:10.1029/2005JD006717, 2006b.

Perez, L., Medina-Ramon, M., Kunzli, N., Alastuey, A., Pey, J., Perez, N., Garcia, R., Tobias, A., Querol, X., Sunyer, J.: Size fractionated particulate matter, vehicle traffic, and case-specific daily mortality in Barcelona (Spain), Environ. Sci. Technol., 43, 4707–4714, doi:10.1021/es8031488, 2009.

Prospero, J. M., Ginoux, P., Torres, O., Nicholson, S. E., and Gill, T.: Environmental characterization of global sources of atmospheric soil dust identified with Nimbus 7 Total Ozone Mapping Spectrometer (TOMS) absorbing aerosol product, Rev. Geophys., 40, 1002, doi:10.1029/2000RG000095, 2002.

Querol, X., Pey, J., Pandolfi, M., Alastuey, A., Cusack, M., Perez, N., Moreno, T., Viana, M., Mihalopoulos, N., Kallos, G., and Kleanthous, S.: African dust contributions to mean ambient PM_{10} mass-levels across the Mediterranean Basin, Atmos. Environ., 43, 4266–4277, ISI:000269095400003, 2009.

Redmond, H. E., Dial, K. D., and Thompson, J. E.: Light scattering and absorption by wind blown dust: theory, measurement, and recent data, Aeolian Research, 2, 1, June 5–26, 2010.

Sakai, T., Nagai, T., Nakazato, M., Mano, Y., and Matsumura, T.: Ice clouds and Asian dust studies with lidar measurements of particle extinction-to-backscatter ratio, particle depolarization, and water-vapor mixing ratio over Tsukuba, Appl. Optics, 42, 7103–7116, 2003.

ACPD
13, 31363–31407, 2013

Sanchez, M. L., García, M. A., Perez, I. A., and de Torre, B.: Ground laser remote sensing measurements of a Saharan dust outbreak in central Spain. Influence on PM_{10} concentrations in the lower and upper Spanish plateaus, Chemosphere, 67, 229–239, 2007.

Sañudo-Wilhelmy, S. A. and Flegal, A. R.: Potential influence of Saharan dust on the chemical composition of the Southern Ocean, Geochem. Geophy. Geosy., 4, 1–3, doi:10.1029/2003GC000507, 2003.

Sassen, K., DeMott, P. J., Prospero, J. M., and Poellot, M. R.: Saharan dust storms and indirect aerosol effects on clouds: CRYSTAL-FACE results, Geophys. Res. Lett., 30, 1633, doi:10.1029/2003GL017371, 2003.

Sawamura, P., Vernier, J. P., Barnes, J. E., Berkoff, T. A., Welton, E. J., Alados-Arboledas, L., Navas-Guzmán, F., Pappalardo, G., Mona, L., Madonna, F., Lange, D., Sicard, M., Godin-Beekmann, S., Payen, G., Wang, Z., Hu, S., Tripathi, S. N., Cordoba-Jabonero, C., and Hoff, R. M.: Stratospheric AOD after the 2011 eruption of Nabro volcano measured by lidars over the Northern Hemisphere, Environ. Res. Lett., 7, 034013, doi:10.1088/1748-9326/7/3/034013, 2012.

Schulz, M., Prospero, J. M., Baker, A. R., Dentener, F., Ickes, L., Liss, P. S., Mahowald, N. M., Nickovic, S., Pérez, C., Rodríguez, S., Manmohan Sarin, M., Tegen, I., and Duce, R. A.: The atmospheric transport and deposition of mineral dust to the ocean: implications for research needs, Environ. Sci. Technol., 46, 10390–10404, doi:10.1021/es300073u, 2012.

Schuster, G. L., Vaughan, M., MacDonnell, D., Su, W., Winker, D., Dubovik, O., Lapyonok, T., and Trepte, C.: Comparison of CALIPSO aerosol optical depth retrievals to AERONET measurements, and a climatology for the lidar ratio of dust, Atmos. Chem. Phys., 12, 7431–7452, doi:10.5194/acp-12-7431-2012, 2012.

Shao, Y., Raupach, M. R., and Findlater, P. A.: Effect of saltation bombardment on the entrainment of dust by wind, J. Geophys. Res., 98, 12719–12726, 1993.

Smoydzin, L., Teller, A., Tost, H., Fnais, M., and Lelieveld, J.: Impact of mineral dust on cloud formation in a Saharan outflow region, Atmos. Chem. Phys., 12, 11383–11393, doi:10.5194/acp-12-11383-2012, 2012.

Stohl, A.: Computation, accuracy and applications of trajectories – a review and bibliography, Atmos. Environ., 32, 947–966, 1998.

Stohl, A. and Thomson, D. J.: A density correction for Lagrangian particle dispersion models, Bound.-Lay. Meteorol., 90, 155–167, 1999.

ACPD
13, 31363–31407, 2013

Tanaka, T. Y., Kurosaki, Y., Chiba, M., Matsumura, T., Nagai, T., Yamazaki, A., Uchiyama, A., Tsunematsu, N., and Kai, K.: Possible transcontinental dust transport from North Africa and the Middle East to East Asia, Atmos. Environ., 39, 3901–3909, 2005.

Tegen, I. and Lacis, A. A.: Modeling of particle size distribution and its influence on the radiative properties of mineral dust aerosol, J. Geophys. Res., 101, 19237–19244, doi:10.1029/95JD03610, 1996.

Todd, M. C., Bou Karam, D., Cavazos, C., Bouet, C., Heinold, B., Baldasano, J. M., Cautenet, G., Koren, I., Perez, C., Solmon, F., Tegen, I., Tulet, P., Washington, R., and Zakey, A.: Quantifying uncertainty in estimates of mineral dust flux: an intercomparison of model performance over the Bodélé Depression, northern Chad, J. Geophys. Res., 113, D24107, doi:10.1029/2008JD010476, 2008.

Vaughan, M. A., Powell, K. A., Kuehn, R. E., Young, S. A., Winker, D. M., Hostetler, C. A., Hunt, W. H., Liu, Z. Y., McGill, M. J., and Getzewich, B. J.: Fully automated detection of cloud and aerosol layers in the CALIPSO lidar measurements, J. Atmos. Ocean. Tech., 26, 2034–2050, 2009.

Veselovskii, I., Dubovik, O., Kolgotin, A., Korenskiy, M., Whiteman, D. N., Allakhverdiev, K., and Huseyinoglu, F.: Linear estimation of particle bulk parameters from multi-wavelength lidar measurements, Atmos. Meas. Tech., 5, 1135–1145, doi:10.5194/amt-5-1135-2012, 2012.

Wagner, J., Ansmann, A., Wandinger, U., Seifert, P., Schwarz, A., Tesche, M., Chaikovsky, A., and Dubovik, O.: Evaluation of the Lidar/Radiometer Inversion Code (LIRIC) to determine microphysical properties of volcanic and desert dust, Atmos. Meas. Tech., 6, 1707–1724, doi:10.5194/amt-6-1707-2013, 2013.

Wandinger, U., Hiebsch, A., Mattis, I., Pappalardo, G., Mona, L., and Madonna, F.: Aerosols and Clouds: Long-Term Database from Spaceborne Lidar Measurements, Final report, ESTEC, Noordwijk, The Netherlands, 15 pp., 2011.

Winker, D. M., Vaughan, M. A., Omar, A., Hu, Y., Powell, K. A., Liu, Z., Hunt, W. H., and Young, S. A.: Overview of the CALIPSO mission and CALIOP data processing algorithms, J. Atmos. Ocean. Tech., 26, 2310–2323, doi:10.1175/2009JTECHA1281.1, 2009.

WMO Secretariat: WMO Sand and Dust Storm Warning Advisory and Assessment System (SDSWAS) – Science and Implementation Plan 2011–2015, 13 March 2011, Research Department, Atmospheric Research and Environment Branch, World Meteorological Organization, Geneva, Switzerland, 18 pp., 2011.

ACPD
13, 31363–31407, 2013

Zender, C. S.: Quantifying mineral dust mass budgets: terminology, constraints, and current estimates, EOS T. Am. Geophys. Un., 85, 509–512, doi:10.1029/2004EO480002, 2004.
Zender, C. S., Bian, H., and Newman, D.: Mineral Dust Entrainment and Deposition (DEAD) model: description and 1990s dust climatology, J. Geophys. Res., 108, 4416, doi:10.1029/2002JD002775, 2003.

ACPD
13, 31363–31407, 2013

Table 1. Geometrical properties of identified dust layers obtained by PEARL observations and BSC-DREAM8b forecast profiles. The values in bold face and between parentheses correspond to limiting the range below 10 km. The table reports also the linear correlation between the 2 count distributions for each parameter and slope s and intercept i obtained from the linear fit between them.

Quantity	PEARL	BSC-DREAM8b	Linear correlation	Linear fit
Base	2.5 ± 0.7 km	2.3 ± 0.6 km	0.958	i = −0.1 ± 0.8 km s = 1.01 ± 0.04
Top	8.0 ± 2.7 km **(6.3 ± 1.6 km)**	10 ± 4 km **(6.5 ± 1.6 km)**	0.802 **(0.932)**	i = 2.3 ± 1.6 km s = 0.50 ± 0.08 **(i = − 0.5 ± 1.2 km** **s = 0.7 ± 0.1)**
Center of mass	3.5 ± 1.0 km	3.8 ± 1.3 km	0.982	i = 1.5 ± 1.1 km s = 0.90 ± 0.03

ACPD
13, 31363–31407, 2013

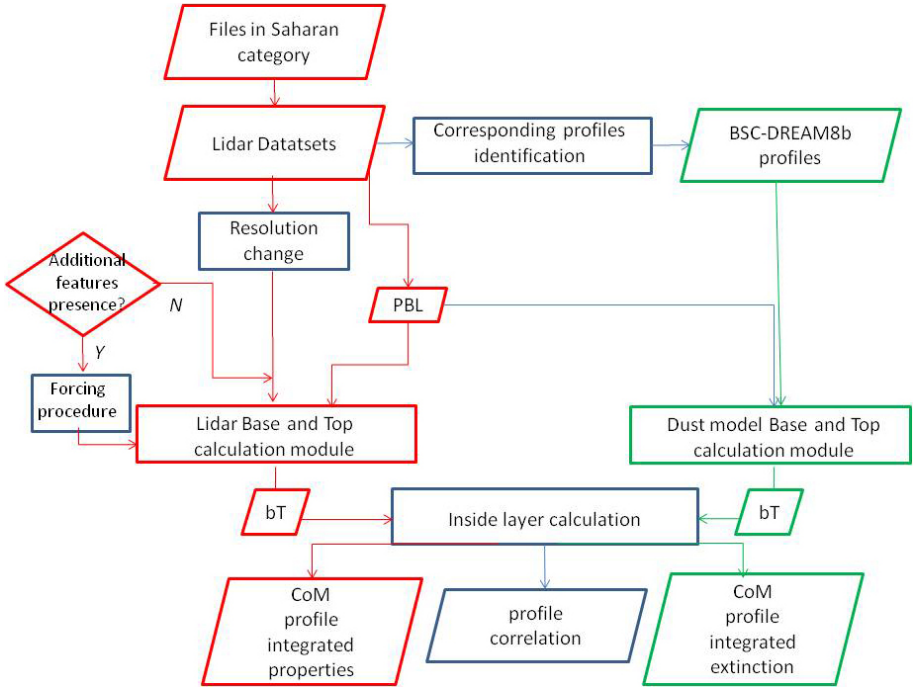

Fig. 1. Flow chart of the comparing methodology software.

ACPD
13, 31363–31407, 2013

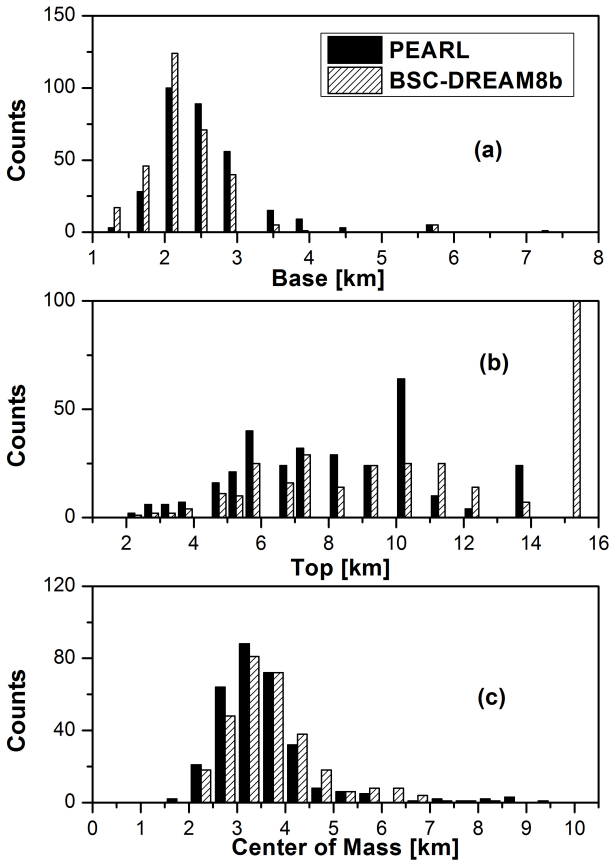

Fig. 2. Counts distribution of the dust layer base **(a)**, top **(b)** and center of mass **(c)** as measured by PEARL lidar and modeled by BSC-DREAM8b.

ACPD
13, 31363–31407, 2013

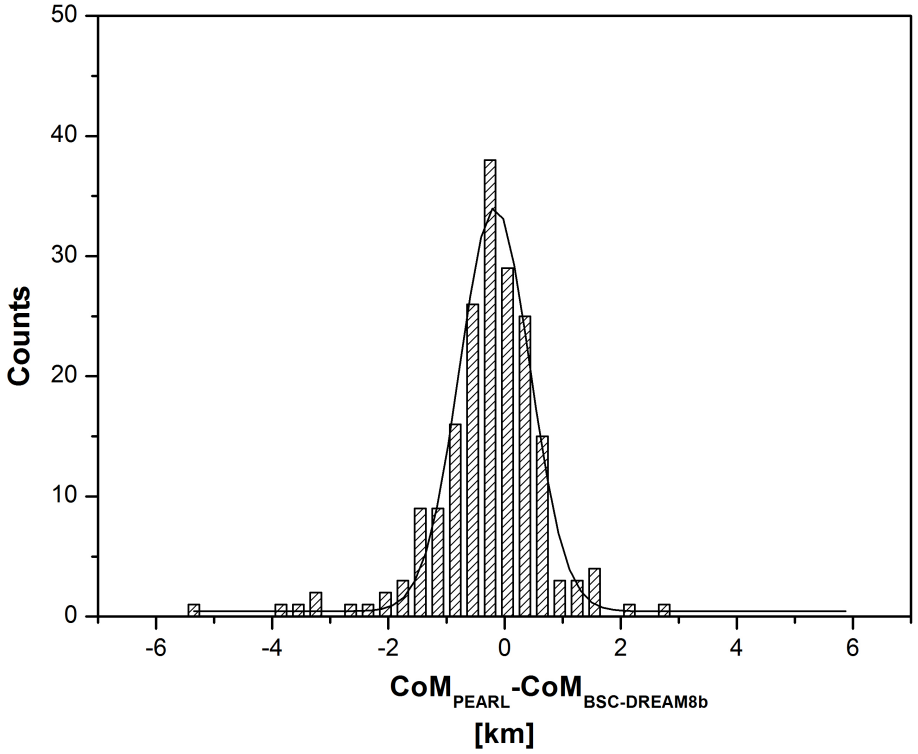

Fig. 3. Counts distribution of the difference of the dust layer CoM as measured by PEARL and evaluated from the BSC-DREAM8b profiles the dust layer.

ACPD
13, 31363–31407, 2013

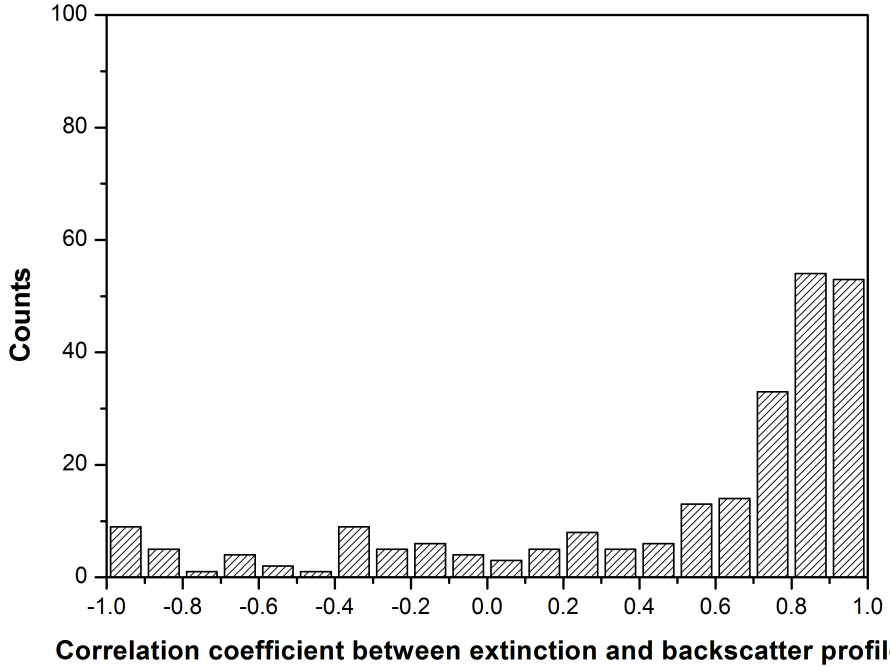

Fig. 4. Counts distribution of the linear correlation coefficient between PEARL and BSC-DREAM8b extinction profiles inside the identified dust layer.

ACPD
13, 31363–31407, 2013

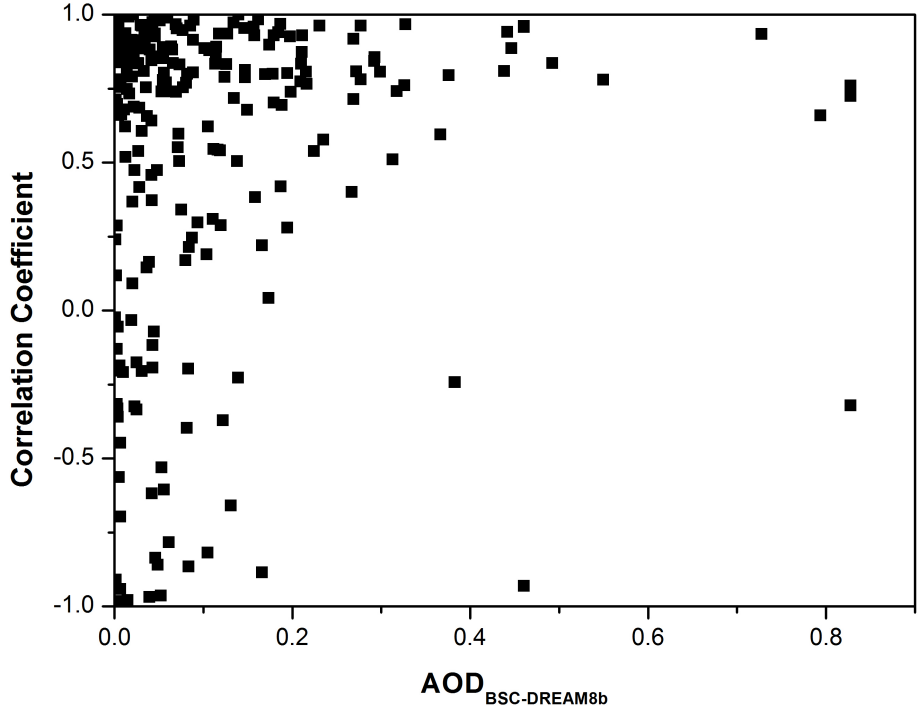

Fig. 5. Linear correlation coefficient between PEARL and BSC-DREAM8b extinction profiles inside the identified dust layer as a function of the aerosol optical depth (AOD) at 500 nm estimated by model profiles.

ACPD
13, 31363–31407, 2013

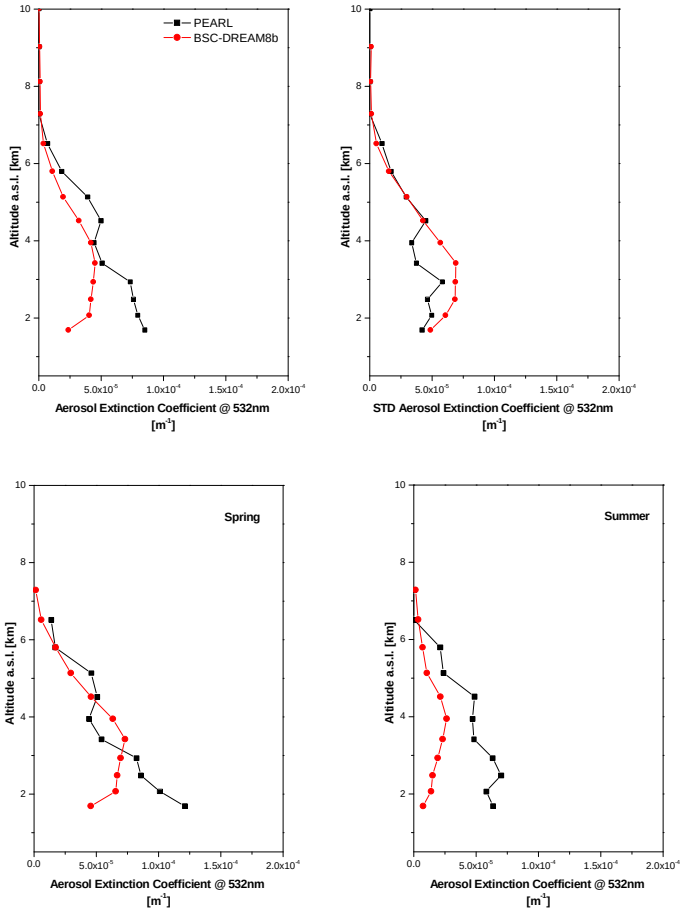

Fig. 6. Mean aerosol extinction profiles (top-left panel) and related standard deviation profiles (top-right panel) calculated for lidar and model within the identified dust layer. Mean aerosol extinction profiles for spring (29) and summer (21) cases are reported in the bottom.

ACPD
13, 31363–31407, 2013

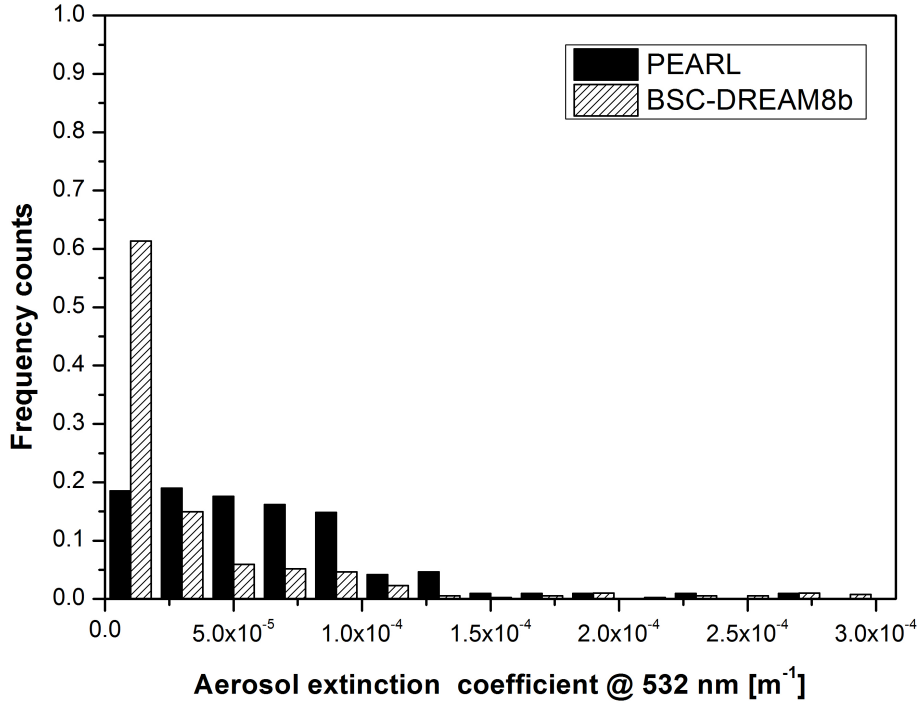

Fig. 7. Counts distribution of the aerosol extinction coefficient as measured by lidar and modeled by BSC-DREAM8b within the dust layer.

ACPD
13, 31363–31407, 2013

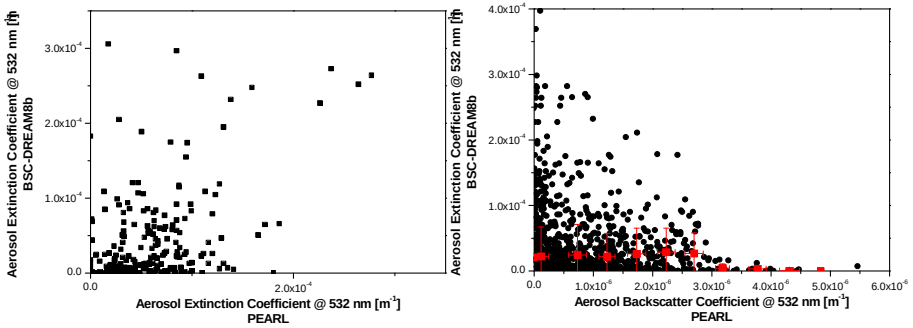

Fig. 8. aerosol extinction coefficient values modeled by BSC-DREAM8b for the dust layer compared to corresponding measured values of aerosol extinction (left panel) and backscatter (right panel). The mean value for backscatter value ranges are also reported in red in the corresponding panel (standard deviations within these ranges are reported as error bars).

ACPD
13, 31363–31407, 2013